Drying Technology
An International Journal
Publication details, including instructions for authors and subscription information:
http://www.informaworld.com/smpp/title~content=t713597247

Modeling of Contact Dryers

Online Publication Date: 01 July 2007
To cite this Article: Tsotsas, E., Kwapinska, M. and Saage, G. (2007) 'Modeling of Contact Dryers', Drying Technology, 25:7, 1377 - 1391
To link to this article: DOI: 10.1080/07373930701439079
URL: http://dx.doi.org/10.1080/07373930701439079

Drying Technology, 25: 1377–1391, 2007

ISSN: 0737-3937 print/1532-2300 online
DOI: 10.1080/07373930701439079

Taylor & Francis
Taylor & Francis Group

Modeling of Contact Dryers

E. Tsotsas, M. Kwapinska, and G. Saage
Thermal Process Engineering, Otto-von-Guericke-University, Magdeburg, Germany

Contact drying of stagnant or agitated beds can be reliably described by the penetration model under vacuum or inert conditions. However, the penetration model has disadvantages in the consideration of granular mechanics and statistics due its continuous nature. The fact that such disadvantages can be avoided by discrete approaches is illustrated by application of the discrete element method to the problem of heating of particles in a rotary drum. Important limiting cases are treated, along with conditions for equivalence between continuous and discrete model. Time constants and scaling aspects are addressed and opportunities of combined product and process engineering are pointed out.

Keywords Agitated bed; Contact drying; Discrete element method; Penetration model

INTRODUCTION

The difference between convective and contact drying is that the energy needed for evaporating the moisture of the product is supplied by a gas phase in the former and by heated apparatus walls or inserts in the latter case. This has serious consequences for the modeling of respective processes. Convective dryer modeling is considered to be a scale-up from single-particle to dryer kinetics by consideration of the spatial distribution and flow of the involved phases, namely solids and gas (see, among many others, Tsotsas[1]). In contrary, contact drying may be regarded as an operation controlled by the efficiency of heat transfer from the wall to the particulate material.[2,3] Since intraparticle kinetics is of minor importance, the task of models is to reliably describe the supply of heat by contact of the assemblage of particles with the hot wall. This task can be accomplished either by continuous or by discrete models. Continuous models that assign effective properties to the bed of particles, especially the penetration model, are the present industrial standard and will, therefore, be discussed first. Then, we will turn our attention to discrete models, which have not yet reached maturity but possess very promising features that let them appear as the upcoming tool for practical applications. The present state-of-the-art and the perspectives will be outlined in close reference to the penetration model.

A thorough comparison between convective and contact dryers in terms of advantages and disadvantages can be found in; e.g., Kemp[4] and Menshutina and Kudra.[5] Here, it should just be mentioned that process intensification (higher evaporation capacity per installed volume) may be one reason for deciding for a contact drying process in practice. Additionally, contact equipment can, in principle, be operated both in presence of inert gas at atmospheric pressure (atmospheric contact drying) or in pure vapor atmosphere at reduced pressure (vacuum contact drying). Furthermore, not only drying but various other mechanical or thermal operations (mixing, granulation, tempering, reaction) can be conducted in contact equipment. This versatility leads to a tremendous variety of constructive configurations and apparatus types (tray, drum, paddle, conical, etc.) with applications for products as divergent as foodstuffs and minerals, chemicals, and drugs. Vacuum drying of beds of crystals containing active pharmaceutical ingredients is covered by the following discussion (compare with Kohout et al.[6]). However, drying of frozen solutions in vials is, with reference to special literature,[7,8] outside of our present scope.

PENETRATION MODEL

Several review articles, books, and handbooks[9–12] summarize the penetration model, developed by Schlünder and coworkers in the years 1975 to 1990. According to it, the time average of the heat transfer coefficient, α, between wall and packed bed can be expressed in a general form as

$$\frac{1}{\alpha} = \frac{1}{\alpha_{ws}} + \frac{1}{\alpha_{bed}} \tag{1}$$

with

$$\alpha_{bed} = \frac{2}{\sqrt{\pi}} \frac{\sqrt{(\rho c \lambda)_{bed,i}}}{\sqrt{t_j}} \cdot f\ (Ph) \tag{2}$$

Correspondence: E. Tsotsas, Thermal Process Engineering, Otto-von-Guericke-University, Universitaetsplatz 2, D-39106 Magdeburg, Germany; E-mail: evangelos.tsotsas@vst.uni-magdeburg.de

Equation (1) combines in series a contact and a penetration resistance, corresponding to the coefficients α_{ws} and α_{bed}. The contact heat transfer coefficient α_{ws} accounts for conduction—and, if necessary, radiation—in the gas gap between wall and first particle layer. Consequently, it depends on gas thermal conductivity and on the average geometrical width of the gap, which can be calculated from the particle diameter, increased by the modified mean free path of the gas molecules in order to capture the influence of pressure (Knudsen effect; see Tsotsas[11,12] for more discussion and precise equations).

Equation (2) is generic in the sense of covering heating or drying of stagnant or mechanically agitated beds in inert or pure vapor atmosphere. This is achieved by adequate assignment of values to the bed properties, the time t_j, and the function f(Ph). Density, ρ_{bed}, specific heat capacity, c_{bed}, and effective thermal conductivity, λ_{bed}, are calculated for the dry bed (i: dry, Table 1) if the bed is really dry and just heated, but also in case of vacuum contact drying. In the latter, a sharp drying front penetrating from the hot wall to the bed is assumed, with heat transfer taking place by conduction before the front (in the dried region of the bed). The dimensionless position of the front is denoted by ζ and depends on the phase change number

$$\mathrm{Ph} = \frac{X\Delta h_v}{c_{bed,dry}(T_w - T_{bed})} \tag{3}$$

and defines the function f(Ph). Respective equations are given in the already cited literature and will, therefore, not be repeated here. However, it is interesting to note that Ph expresses the strength of the latent heat sink present in the bed as the product of solids moisture content, X, and evaporation enthalpy, Δh_v. With increasing Ph, the penetration depth that the front reaches within a certain time decreases, and the penetration heat transfer coefficient α_{bed} increases. At the limit of $\mathrm{Ph} \to \infty$ (very moist solids), $\zeta \to 0$, $\mathrm{erf}\,\zeta \to 0$, $\mathrm{f(Ph)} \to \infty$, $\alpha_{bed} \to \infty$ is obtained, that means the penetration resistance vanishes completely. In contrary, for dry solids ($X \to 0$) it is $\mathrm{Ph} \to 0$, $\zeta \to \infty$, $\mathrm{erf}\zeta \to 1$ and, finally, $\mathrm{f(Ph)} \to 1$. In presence of inert gas, it is assumed that moisture evaporating in the vicinity of the hot wall will recondense completely at the next colder position within the bed, so that no distinct drying front can be established as long as the contact time is relatively short. Hence, $\mathrm{f(Ph)} = 1$ is used in Eq. (2). However, the properties of the wet bed (i: wet, see Table 1) are now applied, and the mechanism of evaporation, diffusion of vapor through the inert gas, and recondensation must be accounted for in the effective thermal conductivity. Due to the requirement of short contact time, stagnant beds must be excluded from this kind of modeling that is applicable only to mechanically agitated beds (Table 1). In total, the agitated bed works like a heat pipe that pumps energy from the heating wall to the bed and from the bed to its interface with the gas phase. Net evaporation takes place only at this interface and can be modeled as usual convective drying (see, again, the literature from Table 1 for details).

Finally, distinction between stagnant and mechanically agitated bed is made by using the real time in the former and the time constant t_R in the latter case in order to calculate the heat transfer coefficient α_{bed} (Eq. (2), Table 1). The time constant t_R is based on the concept of approximating the continuous mixing process with a sequence of static periods, followed by instantaneous and perfect mixing steps, and represents the duration of every such fictitious static period. This is very similar to the penetration or interface renewal theory for gas–liquid mass transfer and gives the model its name. The time constant

TABLE 1
Specification of Eq. (2) for the penetration heat coefficient in a number of practically important cases

Case	i	t_j	f(Ph)	Literature
Heating of stagnant dry bed	Dry	t	1	Wunschmann[31] Muchowski[38] Schlünder[39]
Heating of agitated dry bed	Dry	t_R	1	Wunschmann[31] Schlünder[32]
Vacuum drying of stagnant bed	Dry	t	$1/\mathrm{erf}\zeta$	Mollekopf[17]
Vacuum drying of agitated bed	Dry	t_R	$1/\mathrm{erf}\zeta$	Mollekopf[17] Schlünder and Mollekopf[2] Tsotsas and Schlünder[39] Tsotsas and Schlünder[40] Dittler et al.[41]
Atmospheric drying of agitated bed	Wet	t_R	1	Tsotsas and Schlünder[42] Gevaudan and Andrieu[43] Arlabosse[44]

may be correlated with the revolution frequency of the stirrer or drum, n, according to the relationship

$$t_R = \frac{N_{mix}}{n} \tag{4}$$

that introduces a mixing number N_{mix} as the correlation coefficient.

It should be noticed that correlations are available for calculating the effective thermal conductivity of both dry and wet beds of particles.[12,13] In case of doubt because of unusual particle shape or other reasons, measurements can be conducted quite easily by; e.g., the transient method described by Kwapinski and Tsotsas.[14] A few such measurements can also be used—in combination with the correlation—in order to derive from bed thermal conductivities the unknown thermal conductivity of the particle. After having solved this inverse problem, the correlation can be applied again in the frame of contact drying modeling.

One example of comparison between the previously mentioned operational modes of vacuum and atmospheric contact drying is shown in Figs. 1 and 2. In Fig. 1, vacuum drying curves gained with the help of very small tray equipment (D = 100 mm) and a magnetic stirrer are plotted for two different temperatures of the heating plate. Coarse vacuum had been used, corresponding to a saturation temperature for water of about $T_s = 30°C$, which is equal to the temperature of the bed at the beginning of the process, after a short transient. By just removing the top of the miniature equipment (all other conditions are exactly the same), the results of Fig. 2 are obtained. In Fig. 2b we see that bed temperature is now not fixed by the pressure. Instead, the almost constant values of T_{bed} attained for a long period during the process depend on the interplay between heat supply from the tray and energy consumption by evaporation at the free surface of the bed. The complete penetration model in its respective version must be applied to find such temperatures that turn out to be higher than the previously mentioned 30°C in the present case. As to drying rates, they are reduced to about 50% by letting air into the dryer, as the comparison between Fig. 1 and Fig. 2a shows.

Additional transport resistances, especially mass transfer resistances, may be seen as the reason for this behavior, which, however, must not be generalized. Indeed, the evaporation capacity of atmospheric contact dryers can be increased by both forced convection of the gas phase and additional heat supply from the gas. Such effects were not present in the experiments of Fig. 2, which were conducted with ambient air as the surrounding gas. Following the convention usual for contact drying, drying rates are

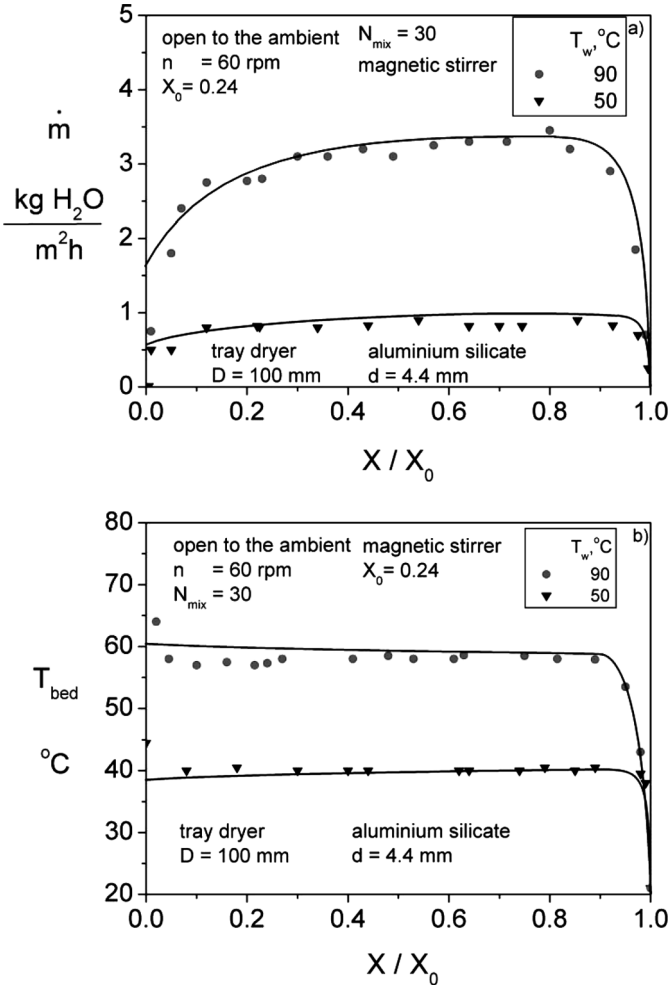

FIG. 2. Contact drying under the same conditions as in Fig. 1, with the only difference of having opened the dryer to the atmosphere. (a) Drying rates, (b) bed temperatures.[42]

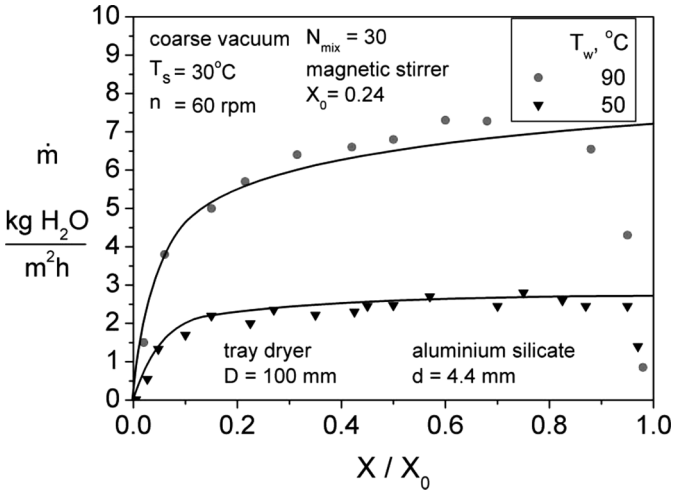

FIG. 1. Contact drying of aluminum silicate under coarse vacuum in a miniature tray dryer.[42]

defined by the heating wall area in contact with the bed in Figs. 1 and 2.

ADVANTAGES OF PENETRATION MODEL

Advantages of the penetration model are seen in:

- Universality and versatility;
- Good performance;
- Appropriate consideration of involved physical phenomena.

The model is universal in providing a frame general enough for enclosing several important cases of application and versatile in considering the particularities of such applications. Its good performance in the comparison with experimental data is documented in the cited literature and should not be further discussed here. However, some examples of the potential of the model to make influences understandable on a physical basis should be given. To this purpose, let us consider the influence of adjustable operating parameters (namely heating wall temperature, stirrer frequency, and pressure) on the drying curve during vacuum contact drying.

An example for the influence of wall temperature has already been given in Fig. 1. Considering the saturation temperature of $T_s = 30^\circ C$, the change of wall temperature from $T_w = 50^\circ C$ to $T_w = 90^\circ C$ in this figure corresponds to an increase of the driving temperature difference for heat transfer by a factor of 3. This results to three times the drying rate at the beginning of the process. The reason for this behavior is that for the large particles used in the respective experiments the contact heat transfer coefficient α_{ws} is small and, therefore, rate controlling ($\alpha \approx \alpha_{ws}$ according to Eq. (1)). Additionally, α_{ws} is (apart from small changes in gas properties and without significant radiation) independent from temperature, so that incoming heat flux and driving temperature difference are directly proportional to each other. The same direct proportionality at the beginning of the process is shown in Fig. 3 for data gained in a larger tray dryer with large particles.

The driving potential is a little bit more than doubled in Fig. 4 by increasing the wall temperature from $T_w = 60^\circ C$ to $T_w = 101^\circ C$. However, less than two times the drying rate are now obtained at the beginning of the process. This is due to the use of small particles in the experiments of Fig. 4. For such particles the contact heat transfer coefficient α_{ws} is large, so that rather the penetration coefficient α_{bed} is rate controlling (it is $\alpha \approx \alpha_{bed}$ according to Eq. (1)). However, and in contrary to α_{ws}, the penetration heat transfer coefficient α_{bed} decreases with increasing wall temperature. The higher the wall temperature, the deeper penetrates the drying front within a certain time and the higher becomes the resistance to further heat penetration.

In this context, the influence of stirrer frequency from Fig. 5 can also be very easily understood. With small

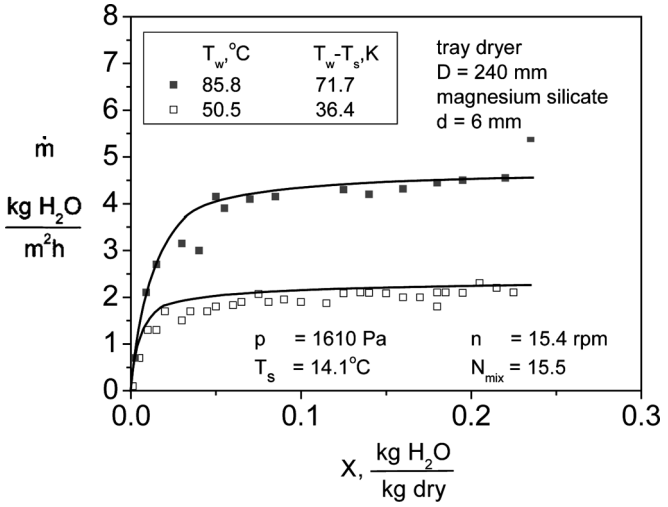

FIG. 3. Influence of wall temperature during the vacuum contact drying of large particles.[17]

particles, the penetration heat transfer coefficient is rate controlling. Since α_{bed} depends on mixing (Eqs. (2), (4), Table 1), an increase of stirrer frequency, n, results to significantly higher drying rates. In contrary, the contact heat transfer coefficient, α_{ws}, that controls the process for large particles does not depend on mixing, so that an increase of stirrer frequency does not pay back. While this is evident at high moisture contents, more precise observation of the data of Fig. 5 reveals that an increase of mixing intensity can make sense even for large particles at low moisture contents. This is not surprising, because with decreasing X the phase change number, Ph, decreases, the penetration depth within a certain time, ζ, increases, the function f(Ph)

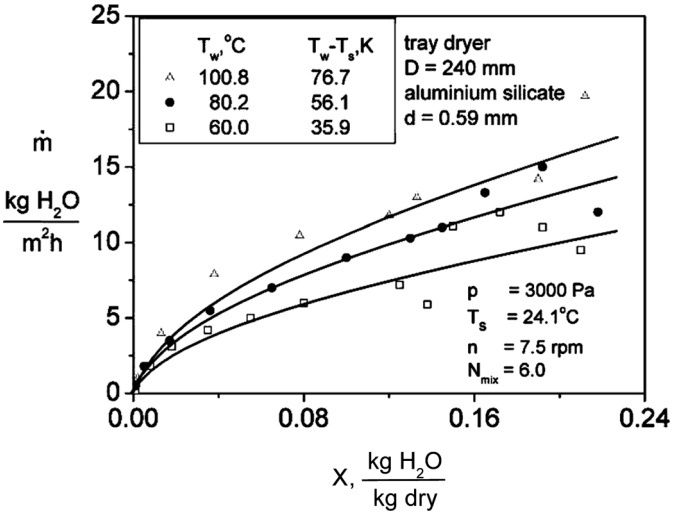

FIG. 4. Influence of wall temperature during the vacuum contact drying of small particles.[17]

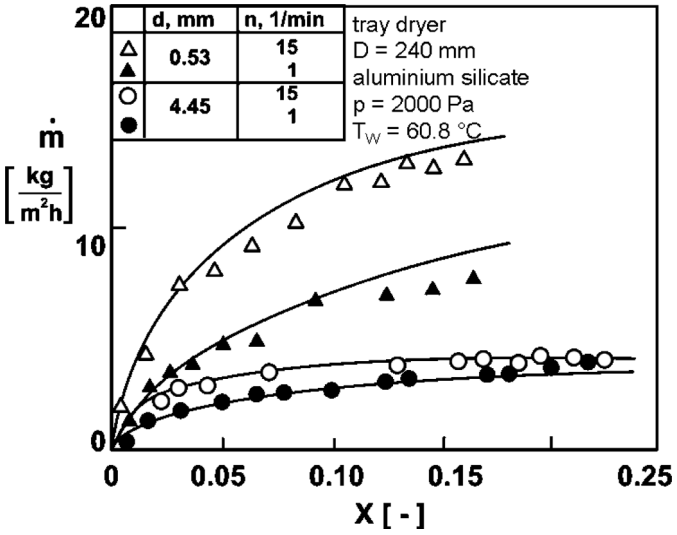

FIG. 5. Influence of stirrer frequency on vacuum contact drying.[45]

decreases and, finally, the penetration heat transfer coefficient α_{bed} also decreases. Therefore, the weight in the series combination is shifted from the contact to the penetration resistance—which is mixing dependent—in the course of drying.

As to the influence of pressure, it is ambivalent. On the one hand, both the contact heat transfer coefficient and the thermal conductivity of the bed, which goes into the penetration heat transfer coefficient, decrease in vacuum. On the other hand, lower pressures mean lower saturation temperatures T_s and, thus, higher temperature differences, $T_w - T_s$, at a constant T_w. While this effect overrules in Fig. 6, the opposite trend is also possible. In fact, pressure is usually selected on the basis of product quality (T_s lower than, e.g., the glass transition temperature)[15] and not of kinetic considerations.

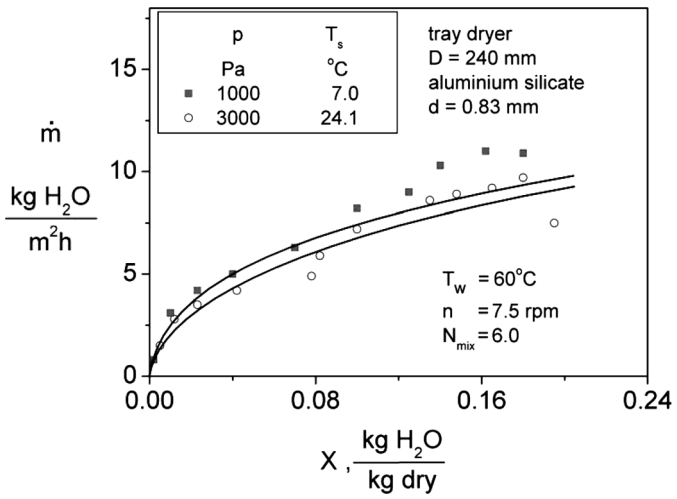

FIG. 6. Influence of pressure on vacuum contact drying.[17]

LIMITATIONS OF PENETRATION MODEL

The most important limitation of the penetration model is that the link to the mechanics of motion of the granular material is missing. Consequently, spatially correlated patterns can be recognized only by additional assumptions,[16] and distributions of particle properties cannot be adequately assessed. Still more important, there is no kind of theoretically founded access to the key parameter of the model, namely the duration of the fictitious static period, t_R, or, in terms of Eq. (4), the mixing number N_{mix}. To overcome this difficulty, correlations of the form

$$N_{mix} = C \cdot Fr^x \tag{5}$$

$$Fr = \frac{(2\pi n)^2\ D}{2g} \tag{6}$$

have been derived by Mollekopf[17] for different types of equipment with the values of C and x as summarized in Table 2. These values are part of handbook recommendations.[11,12] While the idea of such correlations is appealing and its realization by Mollekopf[17] as careful as it could be, it must not be overseen that the amount of data available to him was very limited. In fact, it referred to two tray dryers, two paddle dryers, and just one rotary drum dryer. All of them were operated in the vacuum contact drying modus. Neither the influence of material nor that of stirrer or paddle geometry could be quantified. Data by Mollekopf himself from a tray dryer (some of them appear in Figs. 3, 4, and 6) are well documented and very reliable. However, the few foreign data of industrial origin considered in the development of the mentioned correlations and discussed in his thesis are not available in the open literature.

These are enough reasons for skepticism, leaving the users of the penetration model with the question of how to find values of N_{mix} appropriate for their specific application. The task is by no means trivial, since N_{mix} may depend on the product, it may depend on the stirrer, and it may also depend on both the type and size of the dryer. A few full-scale experiments evaluated by means of the penetration model in order to find N_{mix}, with subsequent computational process optimization, are an evident outcome. Proceeding in such a model-supported way will certainly be faster, cheaper, and more efficient than pure

TABLE 2
Parameters of correlations (Eqs. (5), (6)) for the mixing number

Dryer type	C	x
Tray	25	0.2
Paddle	9	0.05
Rotary drum	16	0.2

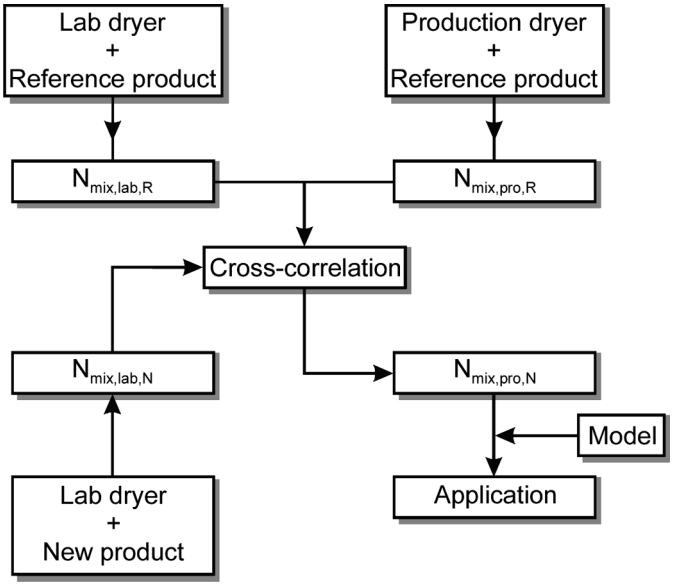

FIG. 7. Scheme for assessing the influence of product change on contact drying without full-scale experiments.

empiricism, but it can still be too expensive or even impossible for products that are either very valuable or simply not yet available in the necessary amount. One possible solution foreseeing only lab-scale experiments with any new product is sketched in Fig. 7, based on the previous establishment of a correlation between the mixing quality in the lab and in the full-scale dryer for a reference product. However, this scheme can only work if such a correlation is invariant upon product change and, even in this case, a new correlation must be derived for every new type or size of production dryer.

From the theoretical point of view, previous authors are well aware of the missing link to granular motion and, therefore, stress that t_R is the time necessary in order to achieve one perfect mixing in the sense of the model; i.e., in order to level out penetrating temperature profiles. The time constant t_R and the respective mixing number N_{mix} (number of revolutions necessary in order to obtain t_R) should not depend on the thermal and thermodynamic parameters of the problem, can, however, not be interrelated or compared with the kinetics of mechanical mixing in the frame of the penetration model.

DISCRETE MODELING

The discussed limitations of the penetration model can be avoided by more rigorous, discrete approaches, namely the discrete element method (DEM). The DEM has the potential of resolving the motion of every individual particle of the bed and, in the thermal version, also calculating the change of temperature due to every particle–particle or particle–wall interaction. Purely mechanical DEM is by now well developed.[18,19] In contrast, only effective thermal properties[20] or gas-borne flows (fluidization,[21] pneumatic conveying,[22] spouted bed[23]) were simulated in the past by thermal DEM. Therefore, an effort aiming at the application of thermal DEM to contact equipment has been started. Respective results[24–28] will be summarized, further analyzed and extended in the present review. These results do not refer to drying, which has not been treated until now, but to the more fundamental problem of heating an agitated bed of spherical particles by contact with an isothermal wall. Additionally, the simplest possible geometry of a two-dimensional rotating drum without inserts, as schematically depicted in Fig. 8, has been chosen. The philosophy of this approach is to systematically proceed from simpler to more complicated cases on the long way towards discrete simulation of realistic contact dryers.

All simulations were conducted with the code PFC^{2D} by ITASCA, which is an upgrade of the discrete element method introduced by Cundall and Strack.[29] In the mechanical part of the code, interactions are treated as a dynamic process with states of equilibrium developing whenever the internal forces are balanced. The contact forces and displacements of an assembly of particles are found by tracing the movement of individual particles. The thermal part of the code associates to each particle a heat reservoir and to the contacts between them a thermal pipe described by power, thermal resistance per length, and length as the distance between centers of touching or overlapping particles. Wall contacts are treated in a similar way. Starting with an initial temperature field, the power in each pipe is updated and reservoir temperatures are calculated by means of the energy balance in discrete form.

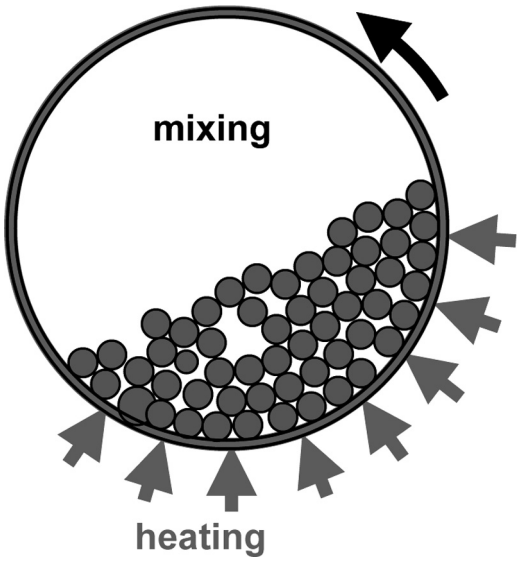

FIG. 8. Sketch of rotary drum simulated by thermal DEM.

The majority of computed data refer to a drum with an internal diameter of $D = 0.25\,m$ and spherical particles with $d = 8\,mm$. The program created the bed by gravitational settling. Drum loadings of 15, 30, and 50% of the total drum volume were simulated, which corresponds to a number of particles of 116, 224, and 370, respectively. The wall temperature was always $T_w = 343\,K$, the initial temperature of the bed $T_0 = 293\,K$. The particle density was set to $\rho_p = 2500\,kg/m^3$. Bed porosities have been evaluated as volume porosities referring to a slab with the thickness of one particle diameter and found to be approximately $\varepsilon = 0.49$. Consequently, the bulk density of the material is obtained to $\rho_{bed} = 1274\,kg/m^3$. In a few simulations, the drum diameter was increased up to a value of $D = 0.54\,m$, which corresponds to 1754 particles, without any further change of parameters.

In the mechanical part of the computations, viscous damping and frictional slip were used to dissipate energy. The critical damping ratio was chosen to 0.16 for particle–particle and 0.07 for wall–particle collisions, which corresponds to restitution coefficients of 0.8 and 0.6, respectively. Friction coefficients of 0.9 were taken between particles, and 0.3 between particles and wall. The elastic response of the particles was assumed to obey a linear contact model, represented by a spring with defined stiffness. The stiffnesses of particles and wall in normal and tangential direction were calculated from the actual mechanical properties of glass particles and steel wall.[30] They have values of $k_n = 3.256 \times 10^6\,N/m$ and $k_s = 2.853 \times 10^6\,N/m$ for the particles and $k_n = 6.799 \times 10^6\,N/m$, $k_s = 5.958 \times 10^6\,N/m$ for the wall.

All simulations with $D = 0.25\,m$ were performed for the rolling mode, with a constant mechanical and thermal time step of $2.0 \times 10^{-6}\,s$. The description of heat transfer requires the thermal time-step to be chosen such that a change in particle temperature does not propagate further than the particle's immediate neighbors within one time step. In the thermal part of the computations, the heat transfer coefficients α_{pp} and α_{pp} describe heat transfer during particle-particle and wall-particle contacts, respectively. The specific heat capacity of the particles corresponds with $c_p = 836\,J/kg\,K$ to that of glass. Since α_{pp} and α_{wp} are treated as free parameters, it is not necessary to specify the kind of gas filling the gaps of the bed. In the same way, it is not necessary to specify the thermal conductivity of the particles.

QUALITATIVE VERIFICATION

Small particle ensembles and the 2D-configuration of Fig. 8 enable relatively fast thermal DEM computations. However, direct comparison with experimental results is not possible, because available experiments were conducted with large particle ensembles in equipment with three-dimensional geometry. This is especially true for the most comprehensive and reliable set of existing heating data, which was gained in a tray device by Wunschmann.[31] Fortunately, the measured data show in a number of limiting cases a very clear and characteristic behavior, so that the results of thermal DEM can be validated in a qualitative way by comparison with this expected behavior. The limiting cases to be distinguished[28] are

- agitated bed with controlling contact resistance;
- stagnant bed;
- agitated bed with controlling penetration resistance.

In every case, the evaluation starts by calculating by thermal DEM the heating curve, which means the average temperature of the bed, T_{bed}, as a function of time, t. Then, time-averaged overall heat transfer coefficients, α, are derived from the relationship

$$\int \frac{dT_{bed}}{T_w - T_{bed}} = \frac{A}{Mc_{bed}}\,\alpha \cdot t \tag{7}$$

with A the heating surface area (wall-bed contact area), M the mass, and c_{bed} the specific heat capacity of the bed, which—for gas–solids systems—is approximately equal to the specific heat capacity of the particles, c_p. Agreement of α with the expected behavior validates the thermal DEM, though indirectly and qualitatively.

The mentioned exercise has been successfully carried out by Kwapinska et al.[27] for the case of contact resistance control, which can be realized experimentally by large particles in vacuum or computationally by much smaller wall–particle than particle–particle heat transfer coefficients ($\alpha_{wp} \ll \alpha_{pp}$; e.g., $\alpha_{wp} = 100\,W/m^2\,K$ and $\alpha_{pp} = 100{,}000\,W/m^2\,K$). The experimental results require in this limiting case a constant value of the heat transfer coefficient α that must be independent from time, drum loading, or mechanical mixing and should be equal to the product of α_{wp} with a reasonable coverage factor, ϕ. These requirements are very well fulfilled by the results of thermal DEM.[27] Additionally, nearly isothermal conditions are predicted within the bed, as one may expect on the basis of the penetration model.

The expected behavior of the heat transfer coefficient to stagnant beds is illustrated in Fig. 9a on the basis of data by Wunschmann.[31] We see:

- Contact control at very short times, which again means a constant value of the heat transfer coefficient. In terms of the penetration model, this value should be $\alpha = \alpha_{ws}$; see Eqs. (1) and (2). In the frame of thermal DEM the relationship

$$\alpha = \phi\ \alpha_{wp} \tag{8}$$

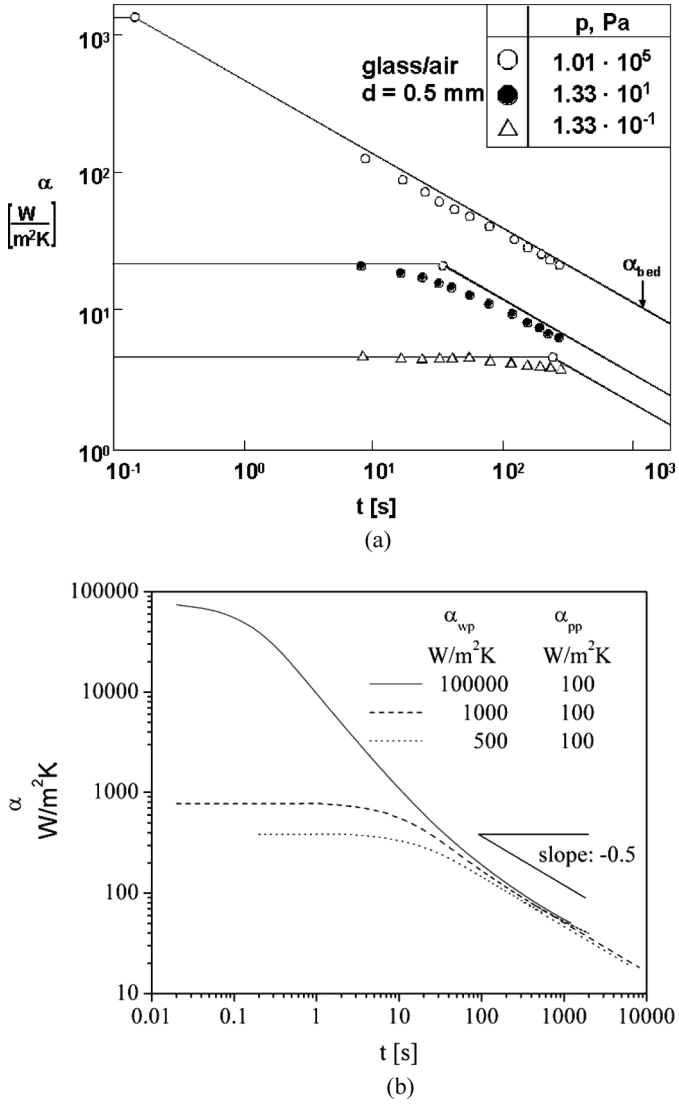

FIG. 9. Heat transfer coefficient to stagnant beds as a function of time: (a) experiments by Wunschmann;[31] (b) results of thermal DEM.

- should be fulfilled, with ϕ the already mentioned surface coverage factor (sum of projections of particles in contact with the wall to the total covered area, A).
- A subsequent decrease of α with time, due to the onset of heat penetration in the interior of the bed.
- The attainment of penetration controlled asymptotes at still longer times. For these asymptotes it holds $\alpha = \alpha_{bed}$ and therefore (Eq. (2), Table 1),

$$\alpha_{bed} = \frac{2}{\sqrt{\pi}} \frac{\sqrt{\rho_{bed} c_{bed} \lambda_{bed}}}{\sqrt{t}} \tag{9}$$

- Notice that the index i = dry is omitted in Eq. (9) and in the following treatment, for the sake of brevity.

The thermal DEM counterpart of Fig. 9a is Fig. 9b. The respective simulations have been conducted with a relative small particle–particle heat transfer coefficient of $\alpha_{pp} = 100\,W/m^2K$ at three different values of the wall–particle heat transfer coefficient α_{wp}. These values can be found again at the beginning of the simulations (short times), though reduced by multiplication with ϕ, according to Eq. (8). The respective values of the surface coverage factor come out to $\phi \cong 0.78$, which is identical to the surface coverage factor obtained in case of contact controlled heat transfer to agitated beds[27] and very reasonable for a random packing of spheres. The higher α_{wp}, the shorter is the contact controlled period—a fact that is reflected in the experimental results and has been analyzed by Schlünder[32] with the help of a critical time corresponding to the intersection point of the asymptotes in Fig. 9a. Beyond such critical times, the results of thermal DEM converge in Fig. 9b irrespectively of the value of α_{wp} to one and the same straight line with the slope -0.5, according to the relationship $\alpha \sim t^{-0.5}$ and in exact correspondence to the behavior of the experimental results and the penetration model (Eq. (9)).

It should be noticed that different long time asymptotes in Fig. 9a are due to the fact that pressure is the parameter of this plot. Different pressures change not only the value of α_{ws} but also the value of α_{bed}, because of changes in the effective thermal conductivity of the bed, λ_{bed} (Eq. (9)). In contrast, the short time behavior can be varied in thermal DEM by variation of α_{wp} without any change in the long time asymptote that is set by α_{pp}. It should also be noticed that all measured data (Fig. 9a) lie in the same stripe of time because of measuring accuracy reasons (influence of the thermal capacity of the heating plate at too short, and of heat losses to the environment at too long times; see Wunschmann[31]). Thermal DEM is not subjected to such restrictions. Finally, it should be stressed that logarithmic plots are essential for clearly discerning the short time behavior, which would be suppressed by the use of linear coordinates.

Since heat transfer coefficients to the stagnant bed depend upon $t^{-0.5}$ at sufficiently long times for both thermal DEM and the penetration model, Eq. (9) can be fitted to the common asymptote of the results of Fig. 9b. This answers the question about the value of the effective thermal conductivity λ_{bed}, which would correspond to the particle–particle heat transfer coefficient α_{pp} used in thermal DEM. For $\alpha_{pp} = 100\,W/m^2K$ and a particle diameter of $d = 8\,mm$ a corresponding value of $\lambda_{bed} = 2.3\,W/mK$ is obtained in this way. The procedure that has been discussed in more detail by Kwapinska et al.[28] establishes an equivalence between continuous and discrete approach, with the invariance of penetration controlled heat transfer to the stagnant bed as the equivalence criterion. The derivation of the functional dependence between α_{pp} and λ_{bed}

may be called calibration. Respective calibration curves can be used in both ways—from a given α_{pp} to λ_{bed} but also from calculated or measured values of λ_{bed} to corresponding values of α_{pp}.

Finally, Fig. 10a shows the behavior of the heat transfer coefficient to mechanically agitated beds according to respective experimental data by Wunschmann.[31] Similarly to the case of the stagnant bed, a contact controlled, common asymptote of all curves can be anticipated at very short times. With increasing time, the value of α decreases, which is also analogous to the findings for stagnant beds. However, constant values of α are attained at still longer times, with a clear dependence upon stirrer frequency and, thus, intensity of mechanical mixing. Exactly the same behavior is observed in Fig. 10b on the results of thermal DEM conducted with $\alpha_{wp} = 100{,}000\,W/m^2\,K$ and $\alpha_{pp} = 100\,W/m^2\,K$. Mechanical agitation does not have any influence at very short times, so that all curves possess one common horizontal asymptote. The respective heat transfer coefficient counts about 80% of the value of α_{wp} due to the surface coverage factor, as already discussed.

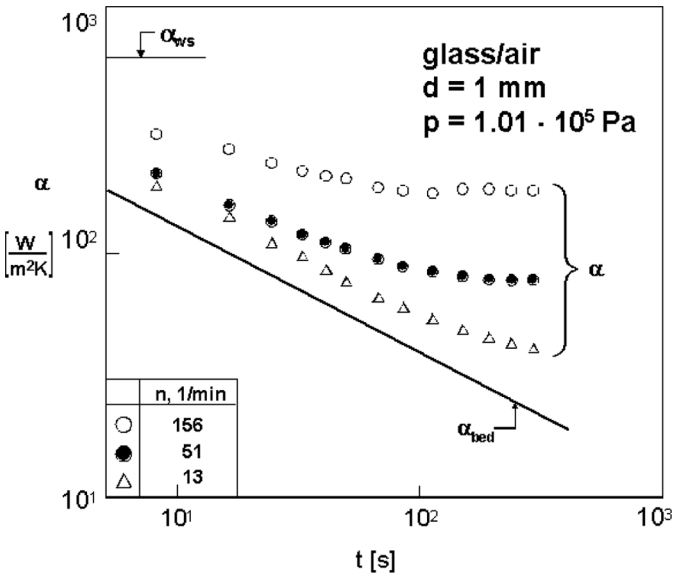

(a)

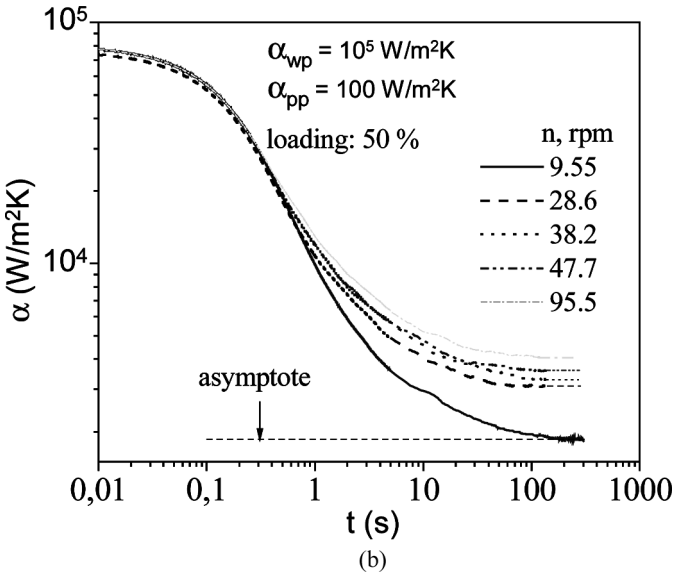

(b)

FIG. 10. Heat transfer coefficient to mechanically agitated beds as a function of time: a) experiments by Wunschmann;[31] (b) results of thermal DEM by Kwapinska et al.[28]

An inhibition of heat transfer is observed with increasing time, with the curves spreading out before reaching new asymptotic values. The higher the revolution frequency of the drum, the higher also this final, quasi-steady-state value of the heat transfer coefficient. Initial and final asymptote would collapse to one flat line in case of perfect mechanical mixing. However, we are far from this limit in Fig. 10b, due to our choice of a very high α_{wp} and, consequently, penetration controlled conditions. It should be noticed that the long-time, quasi-steady-state region is gravely compressed by the logarithmic abscissa in Fig. 10.

TIME CONSTANTS AND THEIR COMPARISON

The long-time, final values of α from Fig. 10b are summarized in Table 3 along with some additional values obtained by Kwapinska et al.[28] at other drum loadings. Then, these values are corrected from the small influence of α_{wp} by setting the right-hand side of Eq. (8) equal to α_{ws} and applying Eq. (1) so that penetration heat transfer coefficients α_{bed} are obtained. In the next step, the version of Eq. (2) applicable to dry, agitated beds, namely

$$\alpha_{bed} = \frac{2}{\sqrt{\pi}} \frac{\sqrt{(\rho c \lambda)_{bed}}}{\sqrt{t_{th,DEM}}} \tag{10}$$

wherein the index i = dry has been omitted and the time t_R has, for better distinction, been renamed to $t_{th,DEM}$, can be used. Inserting in Eq. (2) the effective thermal conductivity of $\lambda_{bed} = 2.3\,W/m\,K$ previously identified by calibration, values of $t_{th,DEM}$ can be obtained. Such values can be considered as time constants of "thermal mixing," which translate the results of thermal DEM into the language of the penetration model by indicating the time necessary for one perfect mixing in the sense of the model. Various interesting comparisons can be carried out at this end.

First, $t_{th,DEM}$ can be compared with the time constant of real mechanical mixing (see also Bridgewater,[33] Malhotra et al.,[34] and Malhotra and Mujumdar[35]), denoted by t_{mech} in Table 3. To derive t_{mech}, separate DEM simulations have been conducted under otherwise the same conditions as previously, though without heat transfer. These purely

TABLE 3
Time constants for heat transfer to agitated beds derived from thermal DEM results with $\alpha_{wp} = 100{,}000\,W/m^2K$ and $\alpha_{pp} = 100\,W/m^2\,K$[28]

		Thermal DEM			PM with tmech		PM			
Rotational velocity (rpm)	Loading (%)	α (W/m^2 K)	α_{bed} (W/m^2 K)	t_{th}, DEM (s)	t_{mech} (s)	α_{bed} (W/m^2 K)	t_{th}, PM (s)	α_{bed} (W/m^2 K)	1/n (s)	$\theta/(2\pi n)$ (s)
28.6	15	2130	2188	0.510	3.5	939.9	21.7	377.5	2.097	0.623
28.6	30	2880	2987	0.247	8.0	621.7	21.7	377.5	2.097	0.815
9.55	50	1870	1914	0.666	39.4	280.1	41.9	271.6	6.282	3.141
28.6	50	3100	3224	0.235	11.7	514.1	21.7	377.5	2.097	1.048
38.2	50	3300	3442	0.204	9.2	579.7	18.3	411.0	1.570	0.785
47.7	50	3590	3758	0.173	7.5	642.1	15.9	440.9	1.257	0.628
9.5	50	4100	4321	0.131	9.8	561.7	10.6	540.1	0.628	0.314

mechanical simulations start with a fully segregated bed of differently colored particles (Fig. 11), track particle mixing by counting the number of contacts between individuals that belong to different fractions, and yield t_{mech} by evaluation of the respective function of time.[26] The result shows that t_{mech} is, in general, not equal to $t_{th,DEM}$. For the specific conditions, the mechanical mixing time is long, and the thermal mixing time is short, as Fig. 12 shows. Whether a cross-correlation might exist between t_{mech} and $t_{th,DEM}$, or not, is an open question.

In Fig. 12, $t_{th,DEM}$ is also compared with the thermal mixing time that can be obtained from Eqs. (4) to (6) with the values of C and x for rotary drum equipment from Table 2, denoted now by $t_{th,PM}$. It should be noticed that the time constant is a very sensitive index of process dynamics. Due to the relationship $\alpha_{bed} \sim t_{th}^{-0.5}$, a change in time constant by a factor of, e.g., four corresponds to a change of α_{bed} by a factor of two (see Table 3), and—in presence of a significant contact resistance—to a still smaller change of α. In spite of this, a large difference between $t_{th,DEM}$ and $t_{th,PM}$ is evident. Too conservative estimation of thermal mixing intensity, which means too high values of $t_{th,PM}$, by the correlation of Mollekopf,[17] may contribute to this deviation.

Apart from the previously discussed uncertainties of this correlation, there is indeed some evidence based on additional, unpublished industrial data for an overestimation of $t_{th,PM}$ in case of rotary equipment. On the other hand, it is also evident from Fig. 12 that correlation and thermal DEM predict almost the same influence of rotational frequency, n, on the time constant, namely $t_{th} \sim n^{-0.6}$ or $N_{mix} \sim n^{0.4}$ in terms of N_{mix}. This means that the mixing efficiency of one revolution decreases with increasing revolution frequency, which is a quite reasonable result.

At the other end, the values of $t_{th,DEM}$ are indeed very small as pointed out by their comparison in Table 3 and

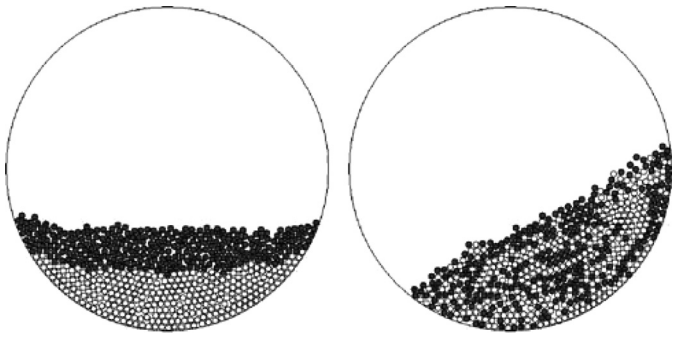

FIG. 11. Example of purely mechanical DEM simulations (initial condition of segregation and rather well-mixed bed of particles after some time).

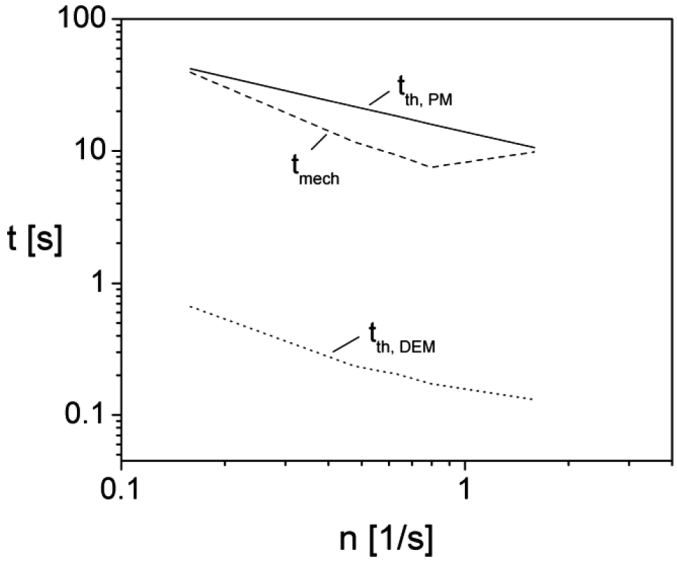

FIG. 12. Thermal mixing times from DEM ($t_{th,DEM}$) in comparison with mechanical mixing times (t_{mech}) and with thermal mixing times derived from existing correlations ($t_{th,PM}$).

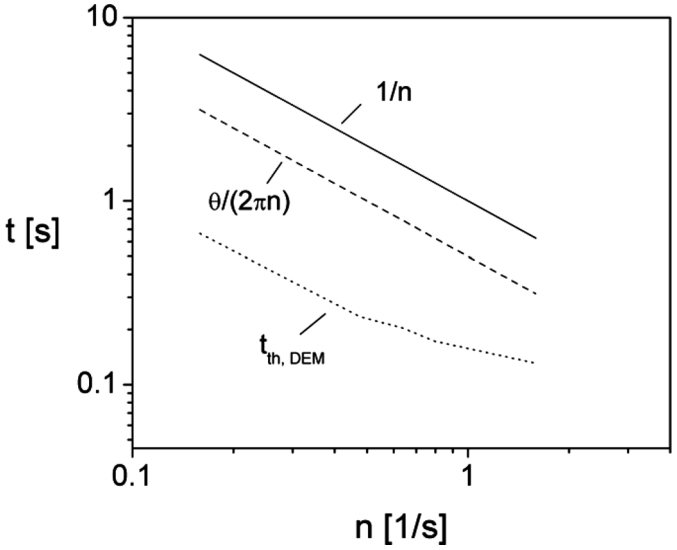

FIG. 13. Thermal mixing times from DEM ($t_{th,DEM}$) in comparison with the natural time constants of the process.

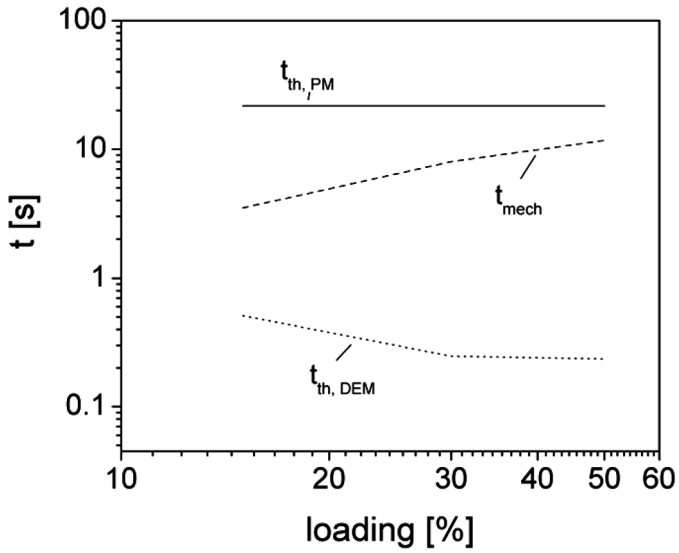

FIG. 15. Influence of drum loading on the time constants.

Fig. 13 with the natural time constants of the considered process, namely $1/n$ and $\theta/(2\pi n)$, where θ is the wall coverage angle. The former is the inverse frequency and would mean one perfect thermal mixing for every revolution of the drum. The latter is the time necessary for one point of the wall of the drum to pass the bed (the covered drum section). As illustrated in Fig. 13, even smaller times are sufficient for perfect thermal mixing according to the results of the discrete model. This appears improbable for industrial size equipment, raising the question about scaling effects in terms of an influence of, e.g., the ratio between drum and particle diameter, D/d. First results of simulations conducted by increasing the drum diameter D with otherwise the same parameters (Fig. 14) indicate the existence of such a scaling effect by higher thermal time constants. However, it should be noticed in connection with Fig. 14 that the flow regime tends to change from rolling to cataracting at about $D/d = 60$, so that one should remain careful with conclusions until more computational data have become available.

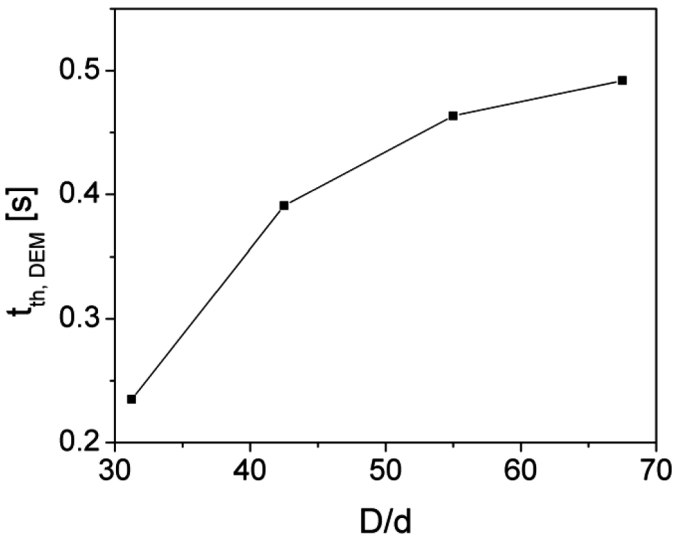

FIG. 14. Scale-up of thermal mixing time with increasing drum diameter, D (45–50% loading, n = 28.6 rpm, smallest $D/d = 31.25$ according to Table 3).

More computational data are necessary also in regard of the influence of loading. As Fig. 15 shows, an increase of loading causes slightly opposing trends in $t_{th,DEM}$ and t_{mech} according to the presently available three simulations from Table 3, while no influence of loading at all is foreseen in the correlations by Mollekopf[17]—in contradiction to, e.g., mechanical data by van Puyfelde et al.[36] Furthermore, three-dimensional thermal DEM simulations are also necessary in order to clarify the possible influence of the third spatial coordinate on the time constants. Respective codes have been applied only to the purely mechanical problem until now.[19]

ADVANTAGES AND LIMITATIONS OF DISCRETE MODELING

The previous discussion shows that we can considerably enhance our knowledge about the interrelation between mixing and heat transfer in contact equipment by means of discrete modeling. Just continuing the described work, an improvement of the correlations available for the time constant of thermal mixing can be expected in respect to both the identification of influential dimensionless quantities and the derivation of fitting parameters. A comparable progress could not be attained in the past two decades

because the penetration model itself does not provide any insight into mixing, and experiments that might contribute this missing link are difficult to conduct, expensive, and, thus, scarce.

While the above advantage rather refers to process engineering, product engineering advantages of the discrete approach are also very significant. To just exemplify respective opportunities, the distribution of particle temperature is depicted in Fig. 16 for one of the simulations from Table 3 in the form of histograms at three different times. We see that the fraction of "cold" particles in the bed is large at $t = 5$ s. However, quite a few particles with a relatively high temperature are present even at this early instant, indicating a fast evolution of the heating process. With increasing time, the distribution is shifted toward higher temperatures. The corresponding temporal change of the variance of the distribution is depicted in Fig. 17. The variance starts at zero (perfectly isothermal bed at $t = 0$), increases rapidly toward an asymmetrically sharp maximum, decreases again, and returns asymptotically to zero as thermal equilibrium is approached and all particles take over the temperature of the wall at the end of the process. This plot would not change fundamentally in case of contact control, though the values of the variance would dramatically decrease.[27,28]

It is easy to anticipate that discrete modeling allows not only for statistics but even for the prediction of the thermal exposition experienced by every single particle in the course of the process. Provided that correlations between thermal exposition and product quality (content or degradation of key components) are available, product quality can be calculated for every individual of the population. In this sense, discrete modeling is the ultimate limit of population dynamics. As in population dynamics, the evolution of product properties—the so-called internal coordinates—can be computed also by discrete modeling, though with the best possible resolution.

Additionally, spatial distributions can also be calculated with the help of thermal DEM, as Fig. 18 exemplifies. Deterministic patterns of particle motion due to the

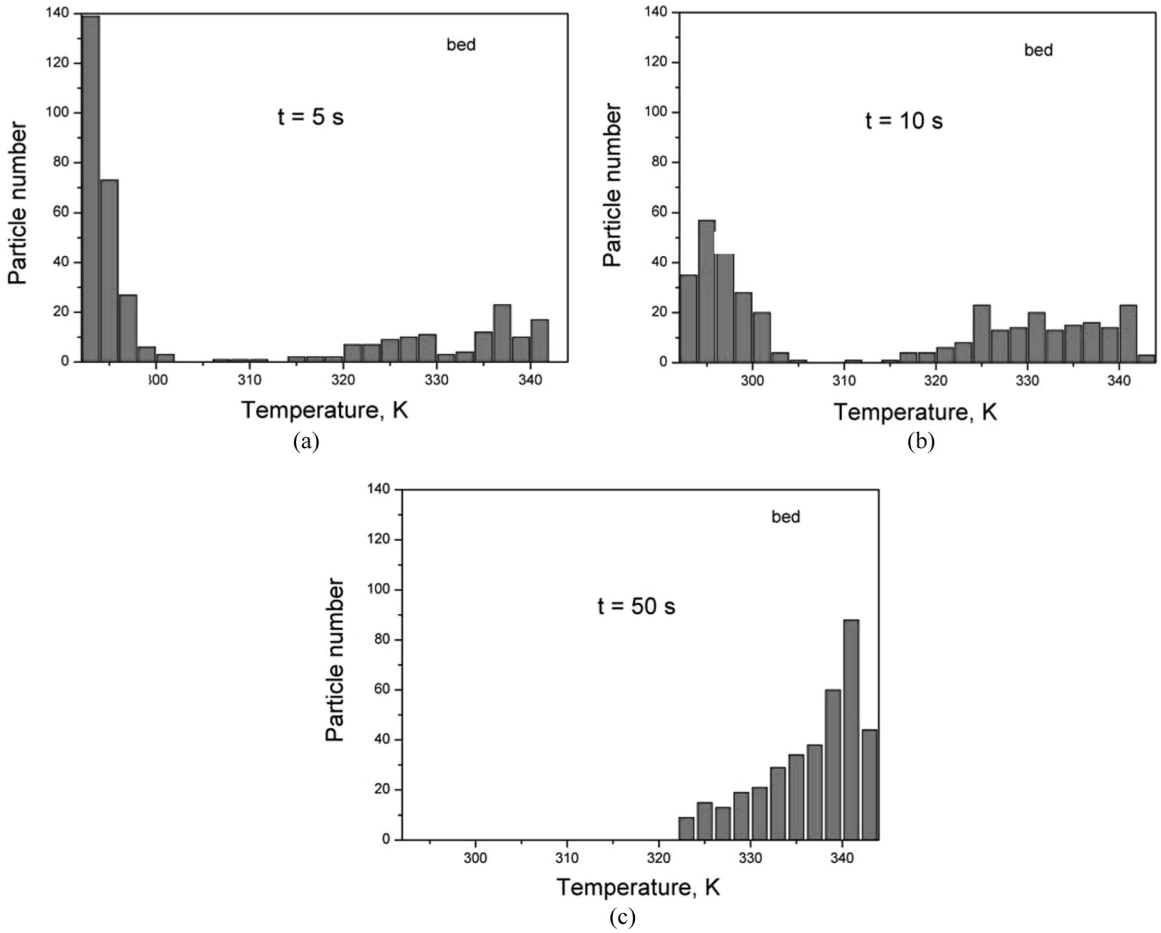

FIG. 16. Distribution of particle temperature at different times in a mechanically agitated bed ($n = 28.6$, loading: 50%, see Table 3) from thermal DEM.

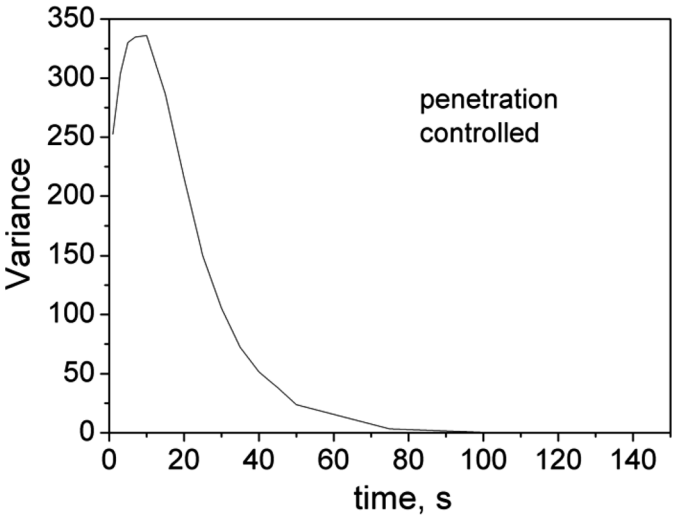

FIG. 17. Variance of temperature distribution as a function of time for the same simulation as in Fig. 16.

geometry and movement of walls and stirrer devices give rise to such spatial distributions, which are not accessible to the standard version of the penetration model.

In the perspective, combined thermo-mechanical processes that involve particle formation (agglomeration, granulation, coating, breakage) and thermal treatment (especially drying) in contact equipment might be approached from the point of view of both process and product engineering. However, respective applications are inhibited by the main drawback of discrete modeling, namely computational time. Computational time is an issue in case of purely mechanical simulations and becomes very critical in the combination of mechanics with heat transfer. In fact, Kwapinska et al.[28] had to invest up to 10 min in order to simulate 1 s of real process time. This is the reason for having started the exploration of applications of thermal DEM to contact equipment with small ensembles of particles, a very simple geometry and high bed thermal conductivities. Therefore, future progress will have to occur in parallel, including, among others, the implementation of discrete modeling for contact drying processes, especially for vacuum contact drying, the incremental improvement of existing codes, and the development of new, multi-scale computational tools that may combine advantages from both the discrete and the continuous modeling. While this is a huge and challenging task, the first available results indicate that it can also be very rewarding in theory and in practice.

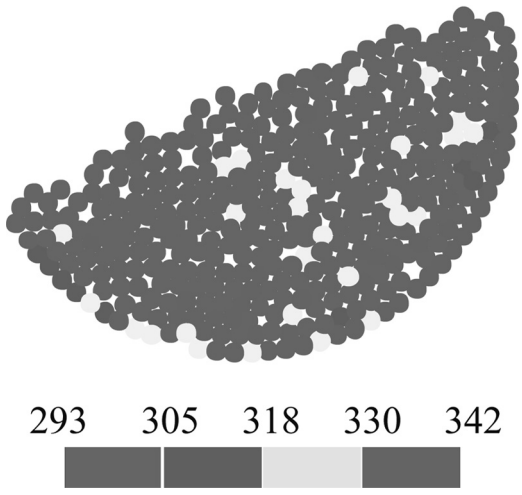

FIG. 18. Example of a spatial distribution of temperature in the rotary drum.

CONCLUSIONS

In the present work, the standard model for contact drying, namely the penetration model, has been reviewed in respect to its advantages and disadvantages. Versatility for treating heating or drying of stagnant or agitated beds in vacuum or in inert gas atmosphere, and the successful interpretation of the influence of various operating parameters on a physical basis, are considered to be important advantages, which are illustrated with the help of respective results. Missing links to granular mechanics and statistics of distributed product properties may be seen as the major disadvantages. Both are, in principle, due to the continuous nature of the model and can thus be removed be discrete approaches.

To elucidate this aspect, the first results available on modeling of heat transfer in contact equipment by the discrete element method are reviewed, discussed, and extended. This is done by reference to small particle ensembles in a two-dimensional rotary drum. It is pointed out that thermal DEM leads to the same temporal behavior of heat transfer coefficients as the penetration model at three important limiting cases, namely agitated bed with controlling contact resistance, stagnant bed, and agitated bed with controlling penetration resistance. Since available experimental data show the very same behavior, the agreement indirectly validates the discrete model. Furthermore, time constants are derived. Their comparison points out that mechanical mixing and thermal mixing have different time scales and that the geometrical scale, expressed by the ratio between drum and particle diameter, should not be neglected. As to the influence of drum revolution frequency, the same trend is obtained from both thermal DEM and previous correlations on the basis of the penetration model, though at different absolute levels. Examples for the potential of thermal DEM to provide spatial patterns and property distributions are given and indicate that process and product engineering may tear great profit

from the further development of discrete modeling of contact equipment, specifically of contact dryers. Respective opportunities referring to the treatment of thermosensitive materials, particle formation processes, and thermomechanical problems are summarized along with limitations due to the high computational cost of the method.

NOMENCLATURE

A	Wall-bed contact area (m^2)
C	Factor of Froude number
c	Specific heat capacity ($J\,kg^{-1}\,K^{-1}$)
D	Drum diameter (m)
d	Diameter (m)
Fr	Froude number, Eq. (6)
g	Acceleration of gravity (ms^{-2})
Δh_v	Evaporation enthalpy($J\,kg^{-1}$)
k	Stiffness (Nm^{-1})
M	Mass (kg)
$\dot{m}$	Drying rate ($kg\,m^{-2}\,s^{-1}$)
N_{mix}	Mixing number
n	Drum revolution frequency (s^{-1})
Ph	Phase change number, Eq. (3)
p	Pressure (Pa)
T	Temperature (K)
t	Time (s)
X	Solids moisture content ($kg\,kg_{dry}^{-1}$)
x	Exponent of Froude number

Greek Letters

α	Heat transfer coefficient ($Wm^{-2}\,K^{-1}$)
ε	Porosity
ζ	Dimensionless position of drying front
θ	Wall coverage angle
λ	Thermal conductivity ($Wm^{-1}\,K^{-1}$)
ρ	Density ($kg\,m^{-3}$)
ϕ	Surface coverage factor

Subscripts

bed	For the bed, for heat penetration
DEM	From DEM
dry	Dry
i	Index
j	Index
lab	Lab scale
mech	Mechanical
N	New product
n	Normal
PM	Penetration model
p	Particle
pp	Particle–particle
pro	Production scale
R	Reference product
R	Fictitious static period
s	Tangential
s	Saturation
th	Thermal
w	Wall
wet	Wet
wp	Wall–particle
ws	Wall-to-first-layer
0	Initial

REFERENCES

1. Tsotsas, E. Industrial convective drying: A unit operation on the way to process systems and product engineering. *Proceedings of the European Drying Symposium (EU Drying 03)*, Crete/Greece, September 4–5, 2003; 15–27.
2. Schlünder, E.U.; Mollekopf, N. Vacuum contact drying of free flowing, mechanically agitated particulate material. Chemical Engineering Processing **1984**, *18*, 93–111.
3. Malhotra, K.; Okazaki, M. Contact drying in mechanically agitated granular beds: A review of fundamentals. In *Advances in Drying*, Vol. 5; Mujumdar, A.S., Ed.; Hemisphere: 1992.
4. Kemp, I. Progress in dryer selection techniques. Drying Technology **1999**, *17*, 1667–1680.
5. Menshutina, N.V.; Kudra. T. Computer aided drying technologies. Drying Technology **2001**, *19*, 1825–1850.
6. Kohout, M.; Collier, A.P.; Stepanek, F. Mathematical modeling of solvent drying from a static particle bed. Chemical Engineering Science **2006**, *61*, 3674–3685.
7. Liapis, A.I.; Pikal, M.J.; Brutini, R. Research and development needs and opportunities in freeze drying. Drying Technology **1996**, *16*, 1265–1300.
8. Hottot, A.; Peczalski, R.; Vessot, S.; Andrieu, J. Freeze-drying of pharmaceutical proteins in vials: Modelling of freezing and sublimation steps. Drying Technology, **2006**, 24: 561–570.
9. Schlünder, E.U.; Tsotsas, E. *Wärmeübertragung in Festbetten, durchmischten Schüttgütern und Wirbelschichten*; Thieme: Stuttgart, 1988.
10. Tsotsas, E.; Martin, H. Heat transfer between a wall and gas-solid dispersed systems. International Chemical Engineering **1991**, *31*, 629–641.
11. Tsotsas, E. Heat transfer to gas-solids system: Heat transfer to packed and agitated beds. Section 2.8.3 of *Heat Exchanger Design Update*; Begell House: New York, 2000.
12. Tsotsas, E. Der Wärmeübergang von einer Heizwand an ruhende oder mechanisch durchmischte Schüttungen. Section Mg of *Wärmeatlas*, 9th Ed.; Springer: Berlin, 2002.
13. Tsotsas, E. *Wärmeleitfähigkeit von Schüttschichten*. Section Dee of *Wärmeatlas*, 9th Ed.; Springer: Berlin, 2002.
14. Kwapinski, W.; Tsotsas, E. Characterization of particulate materials in respect to drying. Drying Technology **2006**, *24*, 1083–1092.
15. Pikal, M.J.; Chang, L.; Tang, X. Evaluation of glassy-state dynamics from the width of the glass transition: Results from theoretical simulation of differential scanning calorimetry and comparisons with experiment. Journal of Pharmaceutical Sciences **1984**, *93*, 981–994.
16. Mellmann, J. The transverse motion of solids in rotating cylinders: Forms of motion and transition behaviour. Powder Technology **2001**, *118*, 251–270.
17. Mollekopf, N. *Wärmeübertragung an mechanisch durchmischtes Schüttgut mit Wärmesenken in Kontaktapparaten*; Ph.D. thesis, University of Karlsruhe, 1983.
18. Yang, R.Y.; Zou, R.P.; You, A.B. Microdynamic analysis of particle flow in a horizontal drum. Powder Technology **2003**, *130*, 138–146.
19. Finnie, G.J.; Kruyt, N.P.; Ye, M.; Zeilstra, C.; Kuipers, J.A.M. Longitudinal and transverse mixing in rotary kilns: A discrete element method approach. Chemical Engineering Science **2005**, *60*, 4083–4091.

20. Vargas, W.L.; McCarthy, J.J. Heat conduction in granular materials. AIChE Journal **2001**, *47*, 1052–1059.
21. Kaneko, Y.; Shiojima, T.; Horio. M. DEM simulation of fluidized beds for gas-phase olefin polymerization. Chemical Engineering Science **1999**, *54*, 5809–5821.
22. Li, J.; Campbell, G.M.; Mujumdar, A.S. A numerical study of heat transfer mechanisms in gas-solids flows through pipes using a coupled CFD and DEM model. Drying Technology **2003**, *21*, 1839–1866.
23. Swasdisevi, T.; Tanthapanichakoon, W.; Charinpanitkul, T.; Kawaguchi, T.; Tanaka, T.; Tsuji. Y. Prediction of gas-particle dynamic and heat transfer in two-dimensional spouted bed. Advanced Powder Technology **2005**, *16*, 275–293.
24. Saage, G.; Kwapinska, M.; Tsotsas, E. An analysis of mixing in rotary drums by means of discrete element method and penetration model. *Proceedings of 5th Powders and Grains Conference*, Stuttgart, vol. B, July 18–22, 2005, 837–840.
25. Kwapinska, M.; Saage, G.; Tsotsas, E. On the way from penetration models to discrete element simulations of contact dryers. *Proceedings of XI Polish Drying Symposium*, Poznan, September 13–16, 2005.
26. Kwapinska, M.; Saage, G.; Tsotsas, E. Mixing of particles in rotary drums: A comparison of discrete element simulations with experimental results and penetration models for thermal processes. Powder Technology **2006**, *161*, 69–78.
27. Kwapinska, M.; Saage, G.; Peglow, M.; Tsotsas, E. Discrete modelling of contact heating of particles in rotating drum. *Proceedings of 5th World Congress of Particle Technology*, Orlando, Paper No. 163d, April 23–27, 2006.
28. Kwapinska, M.; Saage, G.; Tsotsas, E. Continuous versus discrete modelling of heat transfer to agitated beds. Powder Technology **2007**.
29. Cundall, P.A.; Strack, O.D.L. A discrete numerical model for granular assemblies. Geotechnique **1979**, *29*, 47–65.
30. Renzo, A.D.; Maio, F.P.D. Comparison of contact-force models for the simulation of collisions in DEM-based granular flow codes. Chemical Engineering Science **2004**, *59*, 524–541.
31. Wunschmann, J. *Wärmeübertragung von beheizten Flächen an bewegte Schüttungen bei Normaldruck und im Vakuum*; Ph.D. thesis, University of Karlsruhe, 1974.
32. Schlünder, E.U. Heat transfer to packed and stirred beds from the surface of immersed bodies. Chemical Engineering and Processing **1984**, *18*, 31–53.
33. Bridgewater, J. Fundamental powder mixing mechanics. Powder Technology **1975**, *15*: 215–236.
34. Malhotra, K.; Mujumdar, A.S.; Imakoma, H.; Okazaki, M. Fundamental particle mixing studies in an agitated bed of granular materials in a cylindrical vessel. Powder Technology **1988**, *55*, 107–114.
35. Malhotra, K.; Mujumdar, A.S. Particle mixing and solids flowability in granular beds stirred by paddle-type blades. Powder Technology **1990**, *61*, 155–164.
36. van Puyfelde, D.R.; Young, B.R.; Wilson, M.A. Comparison of transverse mixing kinetics data obtained from a rolling drum. Powder Technology **2001**, *114*, 264–265.
37. Muchowski, E. *Der Wärmeübergang vom Boden vibrierter Gefässe an Kugelschüttungen bei Atmosphärendruck und im Vakuum*; Ph.D. thesis, University of Karlsruhe, 1977.
38. Schlünder, E.U. Der Wärmeübergang an ruhende, bewegte und durchwirbelte Schüttschichten. VT-Verfahrenstechnik **1980**, *14*, 459–468.
39. Tsotsas, E.; Schlünder, E.U. Vacuum contact drying of free flowing mechanically agitated multigranular packings. Chemical Engineering Processing **1986**, *20*, 339–349.
40. Tsotsas, E.; Schlünder, E.U. Vacuum contact drying of mechanically agitated beds: The influence of hygroscopic behaviour on the drying rate curve. Chemical Engineering and Processing **1987**, *21*, 199–208.
41. Dittler, A.; Bamberger, T.; Gehrmann, D.; Schlünder, E.U. Measurement and simulation of the vacuum contact drying of pastes in a LIST-type kneader drier. Chemical Engineering and Processing **1997**, *36*, 301–308.
42. Tsotsas, E.; Schlünder, E.U. Contact drying of mechanically agitated particulate material in the presence of inert gas. Chemical Engineering and Processing **1986**, *20*, 277–285.
43. Gevaudan, A.; Andrieu, J. Contact drying modeling of agitated porous media beads. Chemical Engineering and Processing **1991**, *30*, 31–37.
44. Arlabosse, P. Measurement and simulation of contact drying of municipal sewage sludge in a batch agitated dryer. *Proceedings of AFSIA/EFCE Drying Conference*, Paris, May 12–13, 2005, 86–87.
45. Tsotsas, E. *Über der Einfluß der Dispersität und der Hygroskopizität bei der Vakuum-Kontakttrocknung rieselfähiger Trocknungsgüter*; Ph.D. thesis, University of Karlsruhe, 1986.